NANO LETTERS

LETTER

pubs.acs.org/NanoLett

Large Integrated Absorption Enhancement in Plasmonic Solar Cells by Combining Metallic Gratings and Antireflection Coatings

Jeremy N. Munday* and Harry A. Atwater

Thomas J. Watson Laboratories of Applied Physics, California Institute of Technology, Pasadena, California 91125, United States

ABSTRACT: We describe an ultrathin solar cell architecture that combines the benefits of both plasmonic photovoltaics and traditional antireflection coatings. Spatially resolved electron generation rates are used to determine the total integrated current improvement under AM1.5G solar illumination, which can reach a factor of 1.8. The frequency-dependent absorption is found to strongly correlate with the occupation of optical modes within the structure, and the improved absorption is mainly attributed to improved coupling to guided modes rather than localized resonant modes.

KEYWORDS: Solar cells, photovoltaics, plasmonics, absorption enhancement, grating

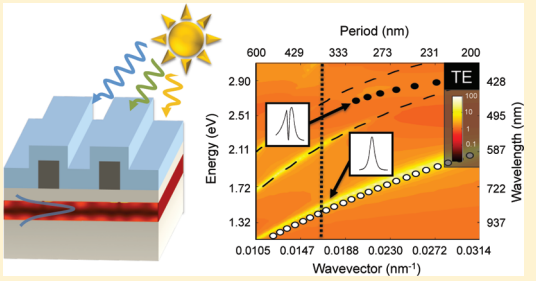

The incorporation of plasmonic scattering structures with photovoltaics has been shown to increase solar cell photocurrent and may lead to new opportunities for inexpensive, high efficiency solar cell designs.[1−3] Experimentally, improved current generation has been found for scattering structures placed on top of,[4−10] within,[11] or on the bottom of[12−14] photovoltaic devices. The earliest experiments with plasmonic particles on top of a photovoltaic device showed photocurrent enhancements of up to 20× over a narrow frequency range,[5] and more recent experiments have shown integrated photocurrent enhancements of ∼7−12% for quantum well structures,[9] c-Si,[8] and GaAs solar cells[10] and ∼33% for silicon-on-insulator devices.[6] Experiments with grating structures have also shown significant enhancements.[15−17] Similarly, results using a variety of full-field electromagnetic simulations and/or semianalytic methods have demonstrated that plasmonic particles can improve incoupling into a semiconducting substrate[3,18] or increase absorption within an absorbing layer with either front[19,20] or back[21,22] textured surfaces or gratings. Photonic and dielectric grating structures have also been shown to improve light absorption.[23−25] Further, once light has been coupled into a waveguide mode, the absorption can exceed the ergodic limit[26] for wavelengths near the band-edge of the semiconductor.[27]

Despite these advances, the question of how plasmonic scatterers compare to traditional dielectric antireflection (AR) coatings is not resolved. Traditional dielectric AR coatings are well suited to reduce reflection at the top interface of a solar cell; however, because there is refraction but not scattering, the incident light cannot be efficiently coupled into waveguide modes, which may be useful for ultrathin film solar cells. Likewise, macroscopic surface texturing that is often used for optically thick solar cells[28] cannot be used on the nanoscale because the films are significantly thinner than the peak-to-valley amplitude of the textured layer.

Here we present a detailed comparison between traditional AR coatings, plasmonic gratings, and structures that combine AR coatings and gratings on ultrathin Si absorbing layers. Plasmonic gratings lead to large, narrow band absorption enhancements, while traditional AR coatings lead to more modest, broad band absorption enhancements. For thicker films, the traditional AR coatings result in more absorption than the gratings alone; however, a combination of gratings and traditional AR coatings surpass the enhancements of either of these structures individually. It is found that the improvement comes mainly from increased absorption within the propagating periodic (Bloch) modes rather than the localized resonances for the structures under consideration.

The reference structure consists of an ultrathin (50−300 nm) Si absorbing layer below a 10 nm thick front surface SiO_2 passivation layer and above an infinitely thick back support substrate of either SiO_2 or Ag. The effect of adding an AR coating or a grating can be determined by comparing the absorption in each structure to the reference structure that has neither an AR coating nor a grating. For structures with an Ag back support, the support can function as an electrical back contact and acts as an optical reflector of the incident light. Because we are interested in the effect of the AR coating or the grating rather than the effect of the back reflector alone, we only compare structures with gratings and AR coatings to reference structures that have similar back support substrates.

Two-dimensional finite difference time domain (FDTD) simulations are used to calculate the absorption within the ultrathin Si slab. Broad band illumination is simulated and the electromagnetic fields are recorded at 100 equally spaced frequencies in the wavelength range of 400−1100 nm

Received: May 27, 2010
Revised: August 21, 2010
Published: October 14, 2010

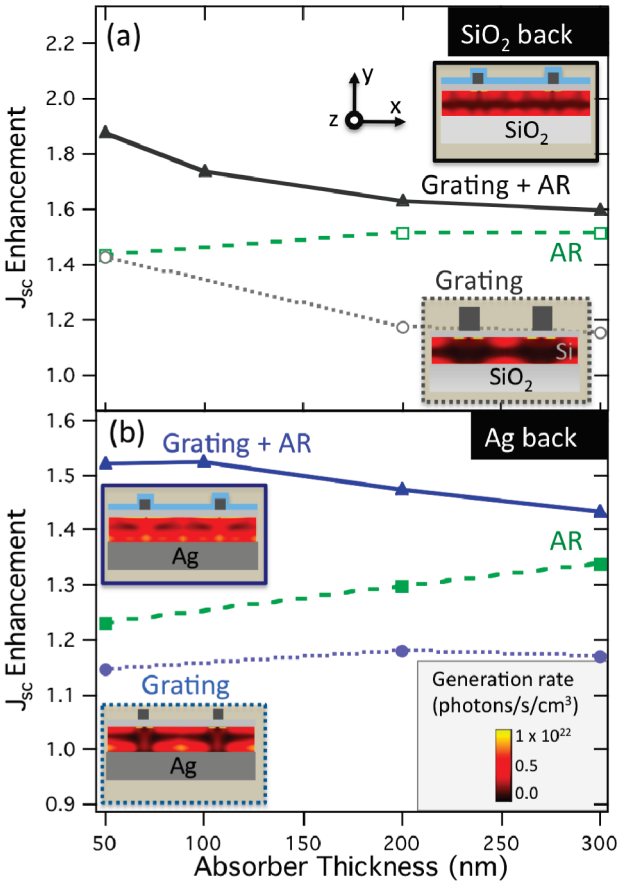

Figure 1. Short circuit current enhancement as a function of absorber thickness for all structures under consideration with either SiO_2 (a) or Ag (b) back support substrates. Structures that combine gratings with conformal AR coatings have current enhancements that surpass the enhancements of either gratings or AR coatings individually. Insets: schematics of structures under investigation and calculated spatially varying electron generation rates.

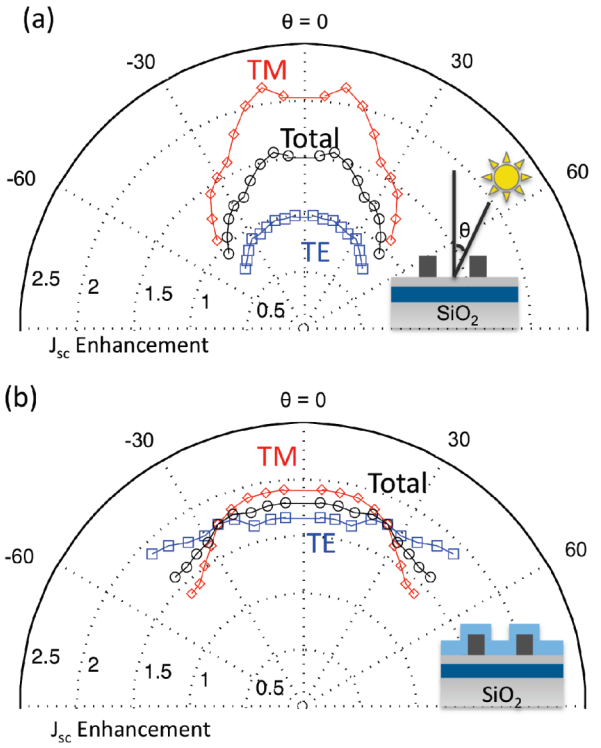

Figure 2. Angular dependence of the integrated current enhancement for (a) a grating structure and (b) a grating structure with a conformal AR coating. Both structures show enhancements for all angles considered, and the grating structure with conformal AR coating gives the largest enhancements with the least angle dependence.

corresponding to above band gap absorption in Si. The results are then weighted by the AM 1.5G solar spectrum. The absorption per unit volume is obtained from the divergence of the Poynting vector as $-(1/2)\mathrm{Re}\,(\vec{\nabla}\bullet\vec{P})$. With the assumption that each photon absorbed within the semiconductor creates one electron−hole pair, the field profiles can be used to calculate the electron generation rate per unit volume

$$GR = \int_{\text{solar spectrum}} \left(\frac{\varepsilon'' |\vec{E}(\omega)|^2}{2\hbar} \right) d\omega$$

where $|\vec{E}(\omega)|^2$ is the magnitude of the electric field squared within the structure resulting from solar illumination and ε'' is the imaginary part of the dielectric function of the semiconductor, which is obtained by a fit to the experimental data of Palik.[29] Note that only absorption that occurs in the Si layer contributes to the generation rate. To isolate the absorption in the Si layer from absorption within the other layers, an index monitor is used and overlaid with the field monitors, as was done in ref 1, 13, and 30. In this way, absorption within the semiconductor, which leads to generation, is separated from absorption within the metal, which leads to Ohmic loss.

The electron generation rates vary spatially throughout the absorbing layer as shown in the insets of Figure 1 for a 50 nm thick Si layer. The reference structures and the structures with AR coatings both have similar generation profiles (not shown); however, the overall rates are higher for the structures with AR coatings and the Fabry−Perot absorption peaks are slightly shifted, as expected. Similarly, the addition of an Ag back reflector results in increased generation at the back of the cell. Structures with gratings show complex generation profiles that vary throughout the simulated region. Here we assume that all generated electrons are collected (i.e., unity internal photocarrier collection efficiency); however, for cases where this is not true, knowledge of the spatially dependent generation rate could also lead to improved designs.

The maximum current is determined under solar illumination for Si layer thicknesses ranging from 50 to 300 nm for structures with gratings, AR coatings, and both gratings and AR coatings as illustrated in Figure 1. We find that the AR coatings generally perform better than the optimized gratings for thicker Si layers; however, for the thinnest absorbing layers, the AR coatings and the gratings become comparable. By conformally coating a grating structure with an AR coating, current enhancements are found that far surpass the enhancements achieved with either gratings or AR coatings individually as seen in Figure 1. For these structures, a conformal AR coating of 45 nm is chosen and the width, height, and period of the gratings are again optimized for maximum current under AM1.5G solar illumination. For all Si absorber thicknesses under consideration, the combined AR-grating structure outperforms the structures with either AR coatings or gratings alone. For the case of a 50 nm Si layer on a SiO_2 support substrate, the AR-grating structure has an enhancement of over 80% when compared to the reference

dx.doi.org/10.1021/nl101875t |Nano Lett. 2011, 11, 2195–2201

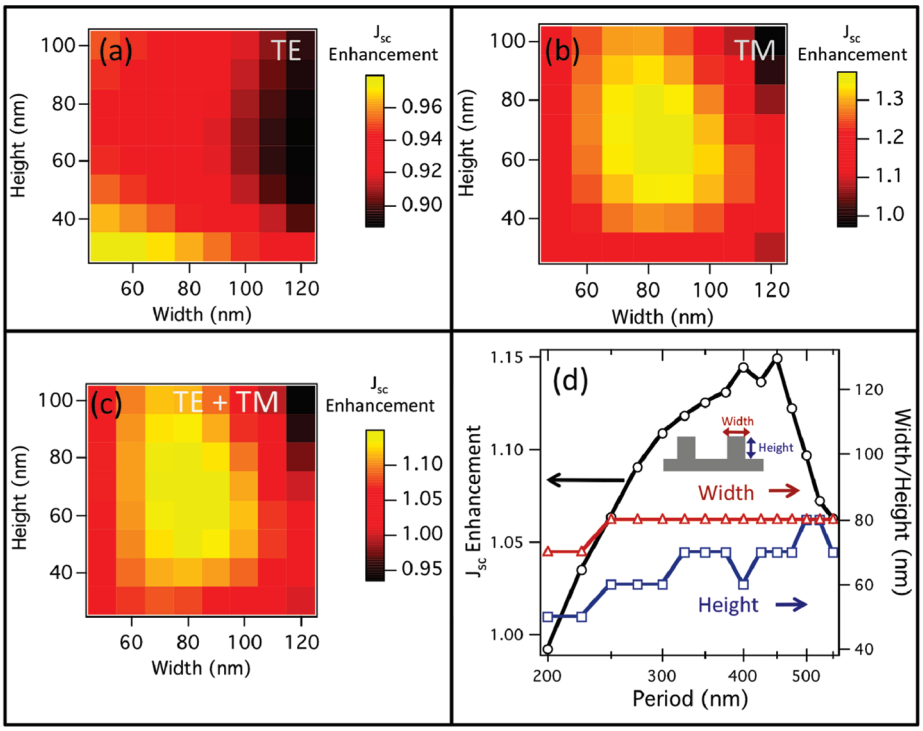

Figure 3. Grating optimization for a 50 nm Si absorbing layer with an Ag back support substrate. Current enhancement as a function of grating height and width for a periodicity of 450 nm is shown for TE (a), TM (b), and TE + TM (c) incident illumination. (d) The widths and heights are varied independently for grating periods ranging from 200 to 550 nm, and the optimal widths and heights are shown for each period.

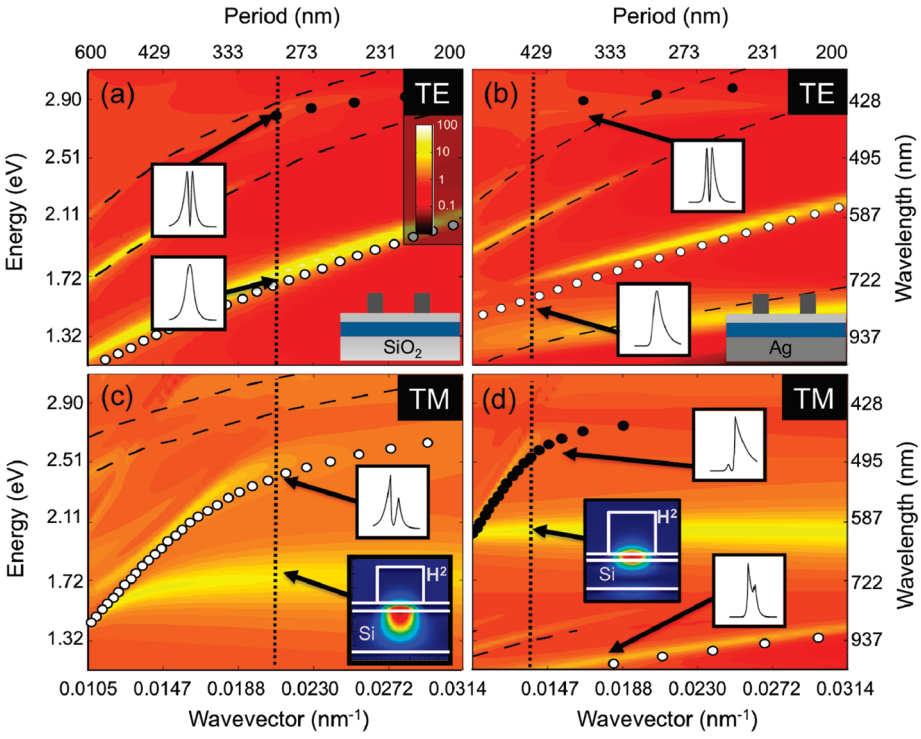

Figure 4. Absorption enhancement (contour plots) and dispersion characteristics (circles and dashed lines) of solar cells with plasmonic gratings. White (black) circles correspond to the lowest order (higher order) propagating waveguide modes, and dashed lines represent repetitions of the lowest order mode with higher periods. The vertical dotted lines denote the periods corresponding to the largest integrated absorption weighted over the solar spectrum. Panels (a) and (c) are for a structure with a SiO_2 back support substrate and a 100 nm (width) by 60 nm (height) grating with periodicity of 300 nm. Panels (b) and (d) are for a structure with an Ag back support substrate and a 80 nm (width) by 70 nm (height) grating with a periodicity of 450 nm. Insets show the 1D mode profiles for propagating modes and the 2D magnetic field intensities for localized resonances found for TM incident light (c and d).

dx.doi.org/10.1021/nl101875t |*Nano Lett.* 2011, 11, 2195–2201

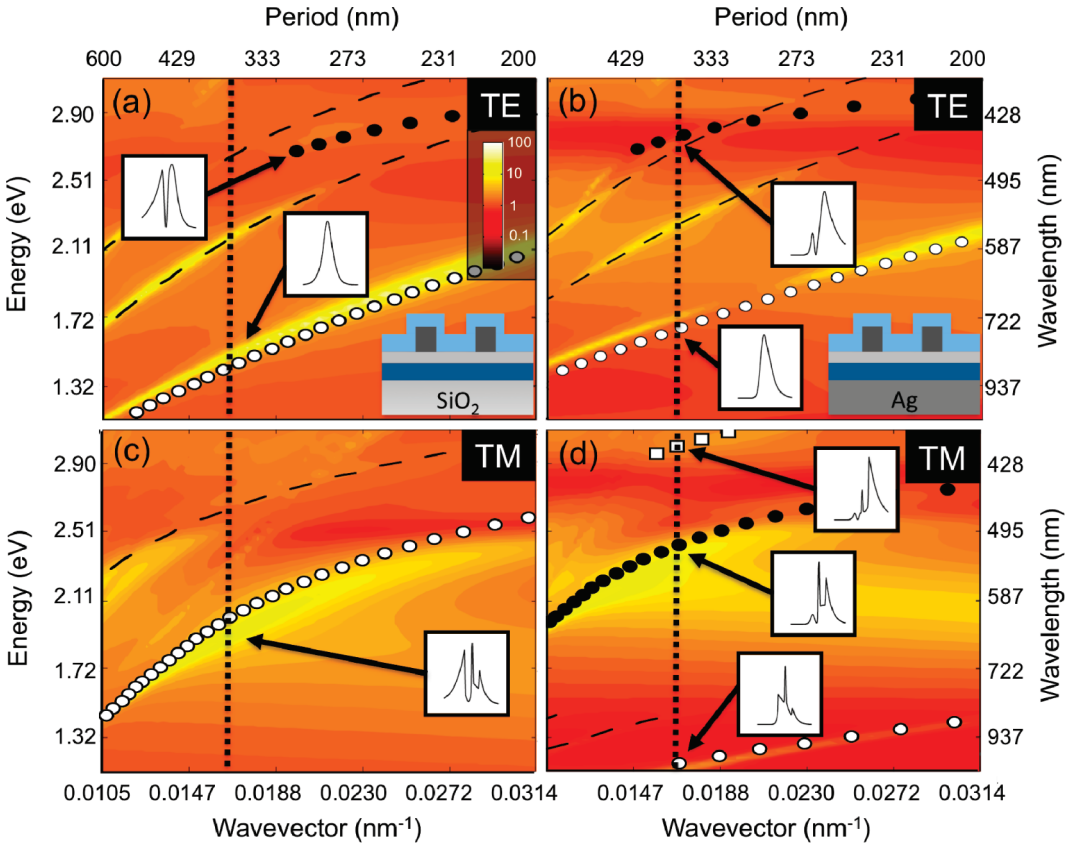

Figure 5. Absorption enhancement (contour plots) and dispersion characteristics (circles, squares, and dashed lines) of solar cells with plasmonic gratings and conformal AR coatings. Mode profiles and dispersion characteristics are slightly modified from Figure 4 due to the AR coating. The grating optimization results in heights and widths significantly smaller than those obtained for structures without AR coatings, which lead to a broadening and blue shifting of the localized resonances (see also Figure 6).

structure and an approximately 30% enhancement over either the AR coating or grating structures individually. Similarly, the AR-grating structure with the Ag support substrate leads to current enhancements of over 50% compared to the reference structure. The angular dependence of the enhancement is also interesting to consider if one wishes to avoid the need for mechanical tracking elements to align the surface normal of the solar cell with the incident light of the sun. Figure 2a shows that the grating alone allows for total current enhancements for angles up to 45°, and Figure 2b shows that the grating structure with a conformal AR coating leads to even larger enhancements, which persist for both polarizations and are less sensitive to the incident angle of illumination.

The optimization procedure is performed by varying the width, height, and period of the grating to determine the maximum possible absorption within the semiconductor. To this end, we calculate the short circuit current per unit area, J_{sc}, for each structure

$$J_{sc} = \frac{q}{A}\int GR\, dV$$

where q is the charge of an electron, A is the illuminated area, and the integration is over the volume which contains generation. Figure 3 shows the result of the grating optimization procedure for a 50 nm thick Si layer with an Ag support substrate normalized to the same structure without the grating. The maximum J_{sc} is found by summing the J_{sc} contributions from both the TE ($\vec{E}$ parallel to the grating) and TM ($\vec{H}$ parallel to the grating) polarizations, because the incident sunlight is unpolarized and thus consists of equal contributions from each polarization. Figure 3d shows the maximum current enhancement as a function of grating period as well as the width and height at which the maximum current enhancement is obtained for each period. The resulting optimized grating structure has a period of 450 nm, width of 80 nm, and height of 70 nm. For the structures with only an AR coating, a thickness of 45−55 nm of Si_3N_4 was found to be optimal above the 10 nm SiO_2 passivation layer using the data of ref 29, which corresponds to an AR dielectric function of $\sim 2.0 + 0.0i$ over the visible spectrum.

Contour plots of the absorption enhancement as a function of 2π/period of the grating strongly resemble waveguide dispersion relations as illustrated in Figures 4 and 5. To confirm this behavior, the modes of a similar waveguide without a grating are solved numerically for each frequency, and the effective mode indices are used to calculate the corresponding wavevectors. Figures 4 and 5 indicate close agreement between the energy and wavevector of calculated dispersion relations and the absorption enhancements for structures with a 50 nm Si absorbing layer. Minor differences are expected to arise because the finite size of the grating perturbs the propagation of the modes. Filled circles correspond to the lowest (white) and higher (black) order propagating modes of the structure. The dashed lines represent repetitions of the lowest order mode with different grating periods, and the vertical dotted lines correspond to the period where the maximum current is found from the optimization

dx.doi.org/10.1021/nl101875t |*Nano Lett.* 2011, 11, 2195–2201

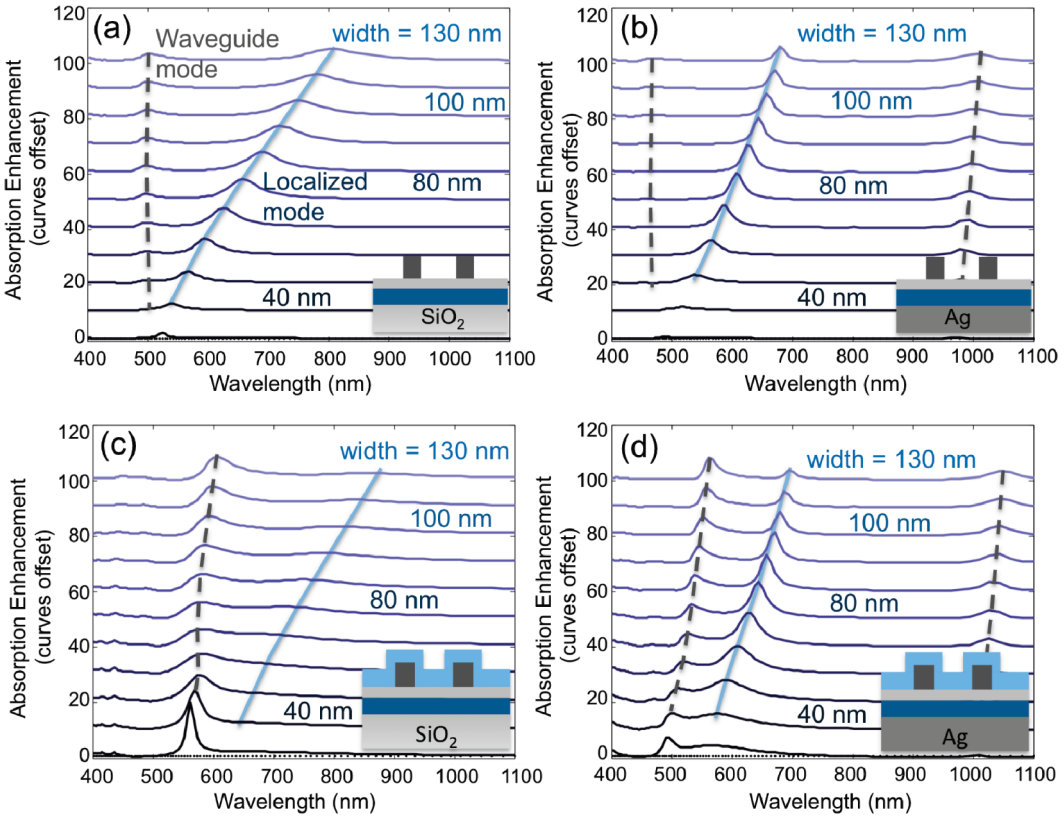

Figure 6. TM absorption enhancement for a grating structure with periodicity of 300 nm and widths ranging from 30 to 140 nm (each curve is offset vertically by 10 for clarity). Dashed (solid) lines are a guide to the eye for the peaks of the waveguide (localized) modes. The addition of an AR coating (c and d) improves the absorption enhancement of the guided mode, while either weakening the localized resonance (c) or leaving it relatively unaffected (d).

procedure. The excited TE modes shown in Figures 4a,b and 5a,b and TM modes shown in Figures 4c,d and 5c,d both lead to coupling of the incident light into waveguide modes (see insets for mode profiles, i.e., E-field intensities within the structure). Differences in the mode profiles between the structure with the SiO_2 back support shown in Figures 4a,c and 5a,c and the Ag back support shown in Figures 4b,d and 5b,d can be seen in the insets as a result of the different boundary conditions at the back interfaces. For the TM case seen in panels c and d of Figure 4, there are two absorption enhancement features that are not explained by the calculated dispersion relations, which do not vary significantly with the grating period. These correspond to the localized surface plasmon resonances of the individual strips that exist at the metal dielectric boundary, as shown by the magnetic field intensities in the insets. For the case of a metallic grating with a SiO_2 support substrate, these results are in agreement with the recently reported work of Pala et al.[19]

The addition of a conformal AR coating to the grating structure only slightly modifies the dispersion relation as shown in Figure 5. However, it causes a dramatic change in the grating optimization and leads to significantly larger current enhancements. As expected, the absorption enhancement is slightly larger for nearly all frequencies as a result of decreased reflection at the top interface. Perhaps what is more surprising is the lack of a strong, isolated surface plasmon resonance under TM illumination. The reason for this is that the optimized structure has a much smaller grating size (40 nm width by 40 nm height for the Ag back support structure and 50 nm width by 40 nm height for the SiO_2 back support structure) and the new dielectric environment changes the localization of the resonance.

To better understand this transition and the relative roles of the localized and guided modes, we consider the frequency-dependent absorption enhancement for the TM polarization with a fixed grating period of 300 nm and height of 40 nm while changing the width of the grating strip from 40 to 140 nm, as in Figure 6. The dashed and solid lines in Figure 6 are a guide to the eye depicting the peak value of the enhancement for the propagating waveguide and localized modes, respectively. The addition of the AR coating in panels c and d of Figure 6 greatly enhances the absorption in the propagating mode for all strip widths; however, the localized resonance is greatly suppressed when the conformal AR coating is applied to the structure with a SiO_2 back support. We believe that this is due to the significantly weaker confinement of the resonance in the Si, as depicted in the insets of panels c and d of Figure 4 which becomes even smaller within the Si when the metallic strip is coated with a dielectric. For the SiO_2 back support structure with a given strip width, the maximum absorption enhancement shifts from being caused by the localized resonance to being caused by the waveguide mode with the addition of the AR coating. It should also be noted that as the grating strip width is reduced, the localized resonance blue shifts and approaches the frequency of the waveguide mode within the structure. This overlap can lead to increased absorption as seen in Figure 6c. For the structure with the Ag back support, the addition of an AR coating does not appear to significantly reduce the absorption caused by the localized surface resonance.

Our analysis can be extended to three dimensions using gratings that have periodicity in two directions, where even

dx.doi.org/10.1021/nl101875t |*Nano Lett.* 2011, 11, 2195–2201

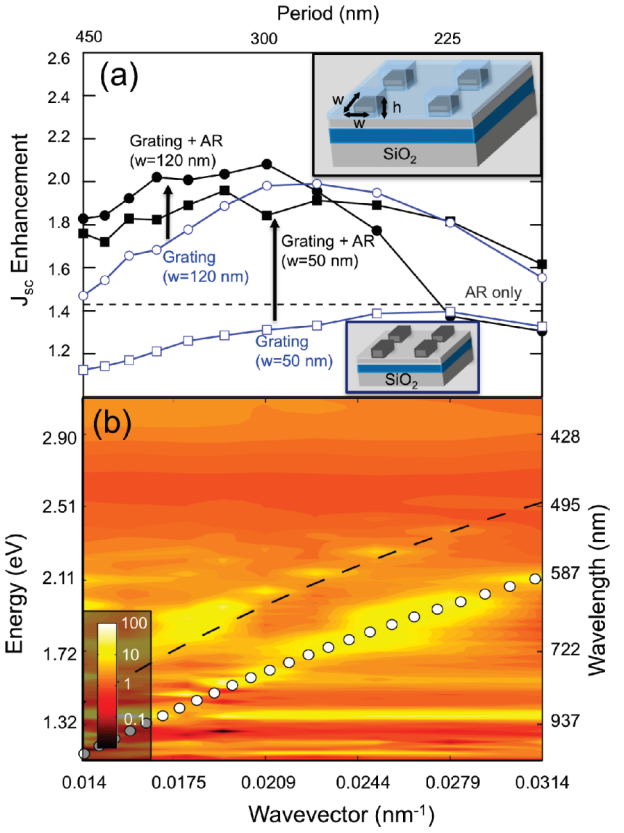

Figure 7. Simulations of AR-coated grating structures with periodicity in two directions show significant absorption enhancements. (a) Current enhancement compared to a reference cell with neither an AR coating nor a grating for four configurations: (i) grating width of 50 nm, (ii) grating width of 120 nm, (iii) grating width of 50 nm with a conformal AR coating, (iv) grating width of 120 nm with a conformal AR coating. (b) Contour plots of absorption enhancements of (iii) with the overlaid dispersion relation (circles) for the lowest order mode of the slab waveguide. The dashed line represents repetitions of the lowest order mode corresponding to periods along the diagonal of the two grating directions. Localized resonances are also visible as bright spots on the contour plot.

larger enhancements can be achieved. As a proof of principle, we have considered two structures: a square array of 50 × 50 × 50 nm^3 Ag scattering objects and an array of 120 × 120 × 50 nm^3 scattering objects (note that these parameters correspond to the previously optimized 2D structures). While a full 3D parameter variation is beyond the scope of this Letter, two main effects can be noted. First, the enhancement cause by a 3D grating structure can surpass the enhancement of a 2D structure (a similar result for a back structured grating coupler was found in ref 31), and second, the addition of a conformal AR coating improves the enhancement cause by the grating alone (see Figure 7). For these 3D structures, the total current enhancement is larger than a factor of 2 and is less dependent on the width of the structure than in the 2D case.

In conclusion, we have performed a detailed analysis of various gratings structures on ultrathin film plasmonic solar cells and found that combining plasmonic gratings with traditional AR coatings can result in large photocurrent enhancements. The addition of an AR coating modifies the optimized grating structure; thus both optimizations should be performed simultaneously. Furthermore, the relative importance of the localized and waveguide modes can change with the addition of an antireflection coating. The dispersion relations for similar waveguides closely resemble the absorption enhancement within the structure; however, the dispersion relations alone do not describe the occupation and useful absorption within the modes. Further optimizations of the dielectric spacer layer, multilayer antireflection coatings or more advanced structures such as "moth-eye" AR coatings,[32] and the consideration of additional three-dimensional scattering structures could lead to even larger enhancements. Alternatively, the ability to spatially predict and modify the generation profiles may be useful in materials where collection of excited carriers is difficult.

AUTHOR INFORMATION

Corresponding Author
*E-mail: jnmunday@caltech.edu.

ACKNOWLEDGMENT

We thank D. Callahan, S. Burgos, E. Feigenbaum, and V. Ferry for helpful discussions. This work was supported by the Department of Energy under Contract DE-FG02- 07ER46405 and the Global Climate and Energy Project (GCEP).

REFERENCES

(1) Ferry, V. E.; Munday, J. N.; Atwater, H. A. *Adv. Mater.* in press; doi: 10.1002/adma.201000488.
(2) Atwater, H. A.; Polman, A. *Nat. Mater.* **2010**, *9* (3), 205–213.
(3) Catchpole, K. R.; Polman, A. *Opt. Express* **2009**, *16* (26), 21793–21800.
(4) Stuart, H. R.; Hall, D. G. *Appl. Phys. Lett.* **1996**, *69* (16), 2327–2329.
(5) Stuart, H. R.; Hall, D. G. *Appl. Phys. Lett.* **1998**, *73* (26), 3815–3817.
(6) Pillai, S.; Catchpole, K. R.; Trupke, T.; Green, M. A. *J. Appl. Phys.* **2007**, *101* (9), No. 093105.
(7) Schaadt, D. M.; Feng, B.; Yu, E. T. *Appl. Phys. Lett.* **2005**, *86* (6), No. 063106.
(8) Matheu, P.; Lim, S. H.; Derkacs, D.; McPheeters, C.; Yu, E. T. *Appl. Phys. Lett.* **2008**, *93* (11), 113108.
(9) Derkacs, D.; Chen, W. V.; Matheu, P. M.; Lim, S. H.; Yu, P. K. L.; Yu, E. T. *Appl. Phys. Lett.* **2008**, *93* (9), No. 091107.
(10) Nakayama, K.; Tanabe, K.; Atwater, H. A. *Appl. Phys. Lett.* **2008**, *93* (12), 121904.
(11) Rand, B. P.; Peumans, P.; Forrest, S. R. *J. Appl. Phys.* **2004**, *96* (12), 7519–7526.
(12) Haug, F. J.; Söderström, T.; Cubero, O.; Terrazzoni-Daudrix, V.; Ballif, C. *J. Appl. Phys.* **2008**, *104*, No. 064509.
(13) Ferry, V. E.; Verschuuren, M. A.; Li, H. B. T.; Schropp, R. E. I.; Atwater, H. A.; Polman, A. *Appl. Phys. Lett.* **2009**, *95* (18), 183503.
(14) Wang, W.; Wu, S.; Reinhardt, K.; Lu, Y.; Chen, S. *Nano Lett.* **2010**, *10* (6), 2012–2018.
(15) Stiebig, H.; Senoussaoui, N.; Brammer, T.; Müller, J. *Sol. Energy Mater. Sol. Cells* **2006**, *90* (18−19), 3031–3040.
(16) Haase, C.; Stiebig, H. *Prog. Photovoltaics* **2006**, *14* (7), 629–641.
(17) Isabella, O.; Campa, A.; Heijna, M.; Soppe, W. J.; Erven, R. v.; Franken, R. H.; Borg, H.; Zeman, M. *23rd European Photovoltaic Solar Energy Conference Proceedings*, 2008
(18) Catchpole, K. R.; Polman, A. *Appl. Phys. Lett.* **2008**, *93* (19), 191113.
(19) Ragip, A. Pala; White, Justin; Barnard, Edward; Liu, John; Brongersma, Mark L. *Adv. Mater.* **2009**, *21*, 1–6.
(20) Akimov, Y. A.; Koh, W. S.; Ostrikov, K. *Opt. Express* **2009**, *17* (12), 10195–10205.

(21) Ferry, V. E.; Sweatlock, L. A.; Pacifici, D.; Atwater, H. A. *Nano Lett.* **2008**, *8* (12), 4391–4397.
(22) Sha, W. E. I.; Choy, W. C. H.; Chew, W. C. *Opt. Express* **2010**, *18* (6), 5993–6007.
(23) Zeng, L.; Bermel, P.; Yi, Y.; Alamariu, B. A.; Broderick, K. A.; Liu, J.; Hong, C.; Duan, X.; Joannopoulos, J.; Kimerling, L. C. *Appl. Phys. Lett.* **2008**, *93* (22), 221105.
(24) Han, S. E.; Chen, G. *Nano Lett.* **2010**, *10* (3), 1012–1015.
(25) Zanotto, S.; Liscidini, M.; Andreani, L. C. *Opt. Express* **2010**, *18* (5), 4260–4274.
(26) Yablonovitch, E.; Cody, G. D. *IEEE Trans. Electron Devices* **1982**, *29*, 300–305.
(27) Saeta, P. N.; Ferry, V. E.; Pacifici, D.; Munday, J. N.; Atwater, H. A. *Opt. Express* **2009**, *17*, 20975–20990.
(28) Green, M. A. *Solar Cells: Operating Principles, Technology and System Applications*; University of New South Wales, 1998.
(29) Palik, E. D. *Handbook of Optical Constants of Solids*; Academic: New York, 1998.
(30) Kelzenberg, M. D.; Putnam, M. C.; Turner-Evans, D. B.; Lewis, N. S.; Atwater, H. A. *Proc. IEEE PVSC, 34th*, 2009
(31) Bermel, P.; Luo, C.; Zeng, L.; Kimerling, L. C.; Joannopoulos, J. D. *Opt. Express* **2007**, *15*, 16986–17000.
(32) Wilson, S. J.; Hutley, M. C. *Opt. Acta* **1982**, *29* (7), 993–1009.